Scanning Electron Microscopy

Volume 1985 | Number 3 Article 14

7-5-1985

Correlation Between Fracture Mechanics Parameters and Fracture Characteristics in Austenites

A. Seibold
Kraftwerk Union AG

R. Löhberg
Kraftwerk Union AG

SCANNING ELECTRON MICROSCOPY/1985/III (Pages 1055-1061)
SEM Inc., AMF O'Hare (Chicago), IL 60666-0507 USA

0586-5581/85$1.00+.05

CORRELATION BETWEEN FRACTURE MECHANICS PARAMETERS AND FRACTURE CHARACTERISTICS IN AUSTENITES

A. Seibold*, R. Löhberg

Kraftwerk Union AG,
Postfach 23 20
8520 Erlangen
West Germany

(Paper received June 16, 1984: manuscript received July 05, 1985)

Abstract

Fracture surfaces of austenitic samples tested at room temperature show a correlation between fracture characteristics, ΔK-value and R-ratio: 1) at low ΔK-values up to 400 $N/mm^{3/2}$ and stress ratios of R = 0.1 and R = 0.7, no fatigue striations but fan-like features and flat facets can be seen; 2) fatigue striations, but no facets exist at ΔK-values greater than 900 $N/mm^{3/2}$ and R = 0.1; 3) at a higher stress ratio of R = 0.7 the facets disappear already at lower ΔK-values of about 650 $N/mm^{3/2}$.

Applied to failure analysis, this correlation permits an estimate of operating level of fatigue stress as a result of the evaluation of fatigue fracture characteristics.

Fracture characteristics of samples tested at 200°C differ from those tested at room temperature, but do not show any appreciable changes in fracture features dependent on the ΔK-value and R-ratio.

KEY WORDS: Fracture Features, Fracture Mechanics, Crack Growth Tests, Austenites, Failure Analysis, Scanning Electron Microscopy.

*Address for correspondence:
Angelika Seibold
Kraftwerk Union AG, Abt. R 411
Postfach 32 20, 8520 Erlangen
West Germany Phone No. (09131) 183341

Introduction

The examination of fracture surfaces under optical or electron microscope is a major element of failure analysis. Characteristic fracture features provide information on whether failure was caused by corrosion and/or mechanical stresses. The defect location in the component and the macroscopic and microscopic characteristics enable the type and orientation of mechanical stresses to be determined.

In failures due to operational stresses, fatigue fractures are a major element. They are caused by unforeseen cyclic loadings which are thus not taken into account in the design of the component. In water-bearing components such loadings may, for example, result from flow conditions giving rise to thermal stressing of the component, or from resonant excitation of the component.

The source of the cyclic loadings is frequently not established; quantitative determination of stress magnitude during unanticipated operational loadings is impossible. Therefore, fractographers are often asked whether they could - beside the identification of a fracture surface as a fatigue fracture - determine the magnitude of the load sustained from the appearance of the fracture surface.

Some hints that such a "quantitative fractography" is possible were found in the literature describing the fracture appearance of samples tested under different conditions to investigate the crack growth behaviour. So it was found that: 1) fatigue striations do not form at low crack growth rates and low ΔK-values /6/, /10/; 2) the appearance of the fatigue striations depends on the material, test frequency and stress magnitude /1/; 3) under certain circumstances one load cycle corresponds to one fatigue striation /7/, /9/; 4) crack propagation rate /5/ and fractographic appearance /2/, /11/ change under the effects of various environments; 5) a correlation exists between heat treatment, stress intensity factor and morphology of the fatigue fracture surfaces in low-alloy steels /4/.

The purpose of the investigation described below was to evaluate systematically the correlation between fracture appearance and test conditions as a basis for "quantitative

fractography" on austenites. As for the part of the investigators, "quantitative fractography" is to be applied on fatigue fractures in components which are exposed to water of varying temperature (room-temperature to about 300°C) during operation; these conditions were taken into account during test performances.

Test performances

Fractographic examination was performed on austenitic fracture surfaces produced by loading in the tension-tension stress range, varying test frequency, temperature, stress ratio and environment. The tests were conducted as crack growth tests and three-stage tests. While in the crack growth tests the ΔK-value increases continuously with crack depth; three different ΔK-values (350, 550 and 850 N/mm$^{3/2}$) were held constant at specific crack depths in the three-stage test.

Reference images of fracture features which were typical for a certain test condition were compiled in a catalog.

The test parameters are listed below.

Material

Austenite X 10 CrNiNb 18 9 (German Standard Nr. 1.4550, USA grade TP 347). Chemical analysis (German Standard DIN 17440):
C $\leq$ 0.1 wt.%, Si $\leq$ 1.0 wt.%, Mn $\leq$ 2.0 wt.%, Cr 17 - 19 wt.%, Ni 9 - 11.5 wt.%, Nb $\geq$ (8 x wt. %C).

Specimens

For the description of WOL 25 X-samples see /12/.

Test Parameters

Room temperature tests in air:
Test frequency: 100 Hz
Stress ratio: $R = \frac{\text{min}}{\text{max}} = 0.1$

Room temperature tests in demineralized water:
Test frequency: 1, 10 and 100 Hz
Stress ratio: R = 0.1 and R = 0.7

Tests at 200°C, demineralized water, 30 bar, 200 ppb O_2:
Test frequency: 0.1 Hz
Stress ratio: R = 0.2 and R = 0.7

Test results

Crack Growth Rate

Evaluation of the crack growth tests and three-stage tests at room temperature yields the following results: 1) at a frequency of 100 Hz and a stress ratio of R = 0.1 the crack growth rate does not depend on the test environment; 2) reduction of the frequency to 1 Hz (R = 0.1, demineralized water) causes the crack growth rate to rise (Fig. 1); 3) the crack growth rate (1 Hz, demineralized water) increases with rising stress ratio (Fig. 1).

At the test temperature of 200°C, (0.1 Hz, demineralized water, 30 bar, 200 ppb O_2), however, the crack growth rate was not observed to depend on the R ratio (Fig. 2).

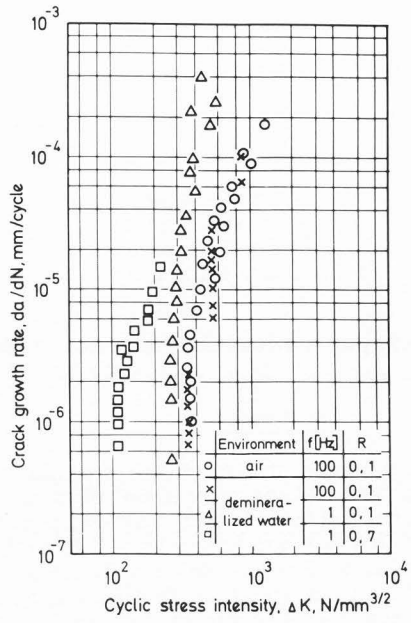

Fig. 1: Correlation between crack growth rate and ΔK at RT

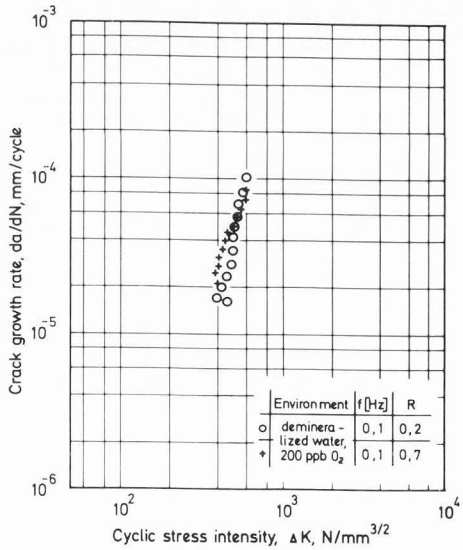

Fig. 2: Correlation between crack growth rate and ΔK at 200°C

Fractographic Examinations

Fractographic evaluation of the fracture surfaces reveals that at room temperature fracture characteristics can be assigned to ΔK-value ranges, which depend on the respective stress ratio, regardless of test frequency and test environment.

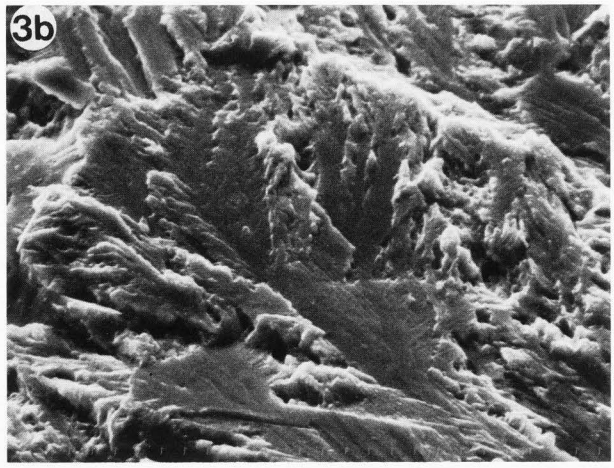

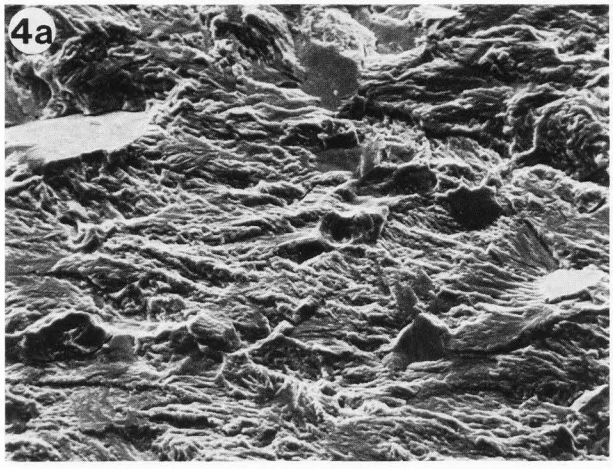

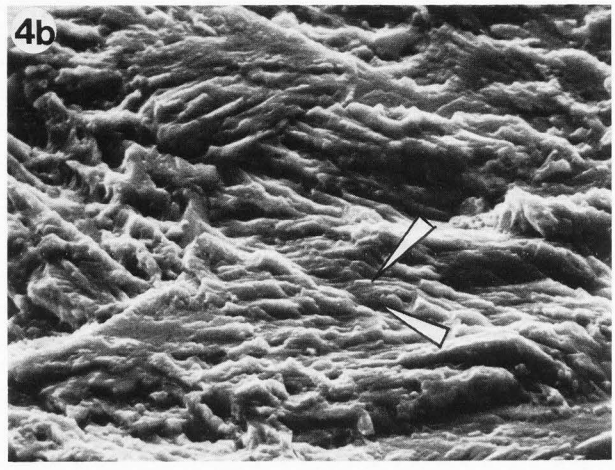

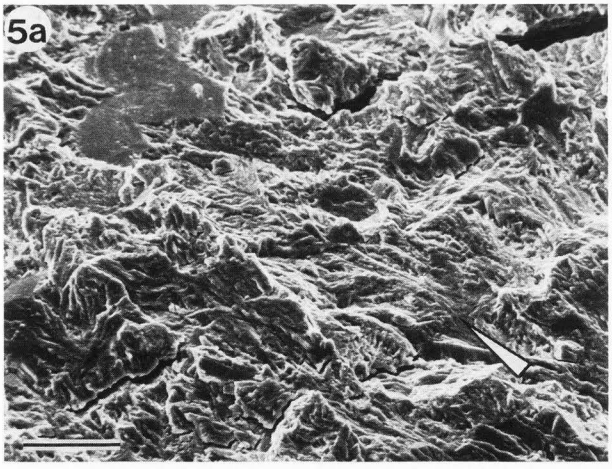

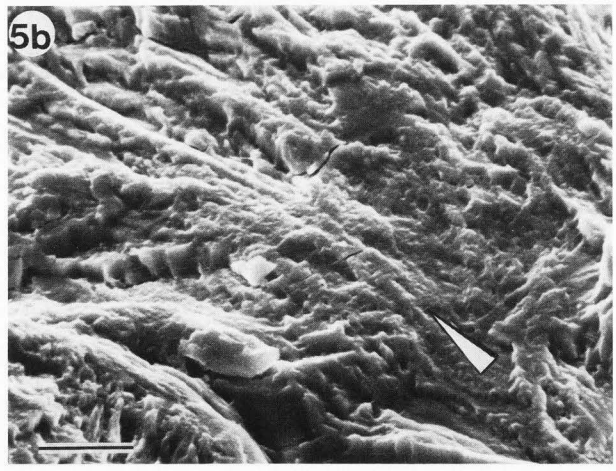

Figs. 3a and 3b: Fans and facets at $\Delta K = 350\ N/mm^{3}/^{2}$, f = 1 Hz.
Figs. 4a and 4b: Roughened fans, facets and fatigue striations (arrows) at $\Delta K = 550\ N/mm^{3}/^{2}$, f = 1 Hz.
Figs. 5a and 5b: Feathered structure, facets, fatigue striations (arrows) and secondary cracks at $\Delta K = 850\ N/mm^{3}/^{2}$, f = 1 Hz.
Figs. 3, 4, and 5: Fracture characteristics as a function of ΔK-value at room temperature and R = 0.1.
Figs. 3a, 4a and 5a are at same magnification, so are figs. 3b, 4b and 5b. Bar = 40 μm in Fig. 5a; 10 μm in Fig. 5b.

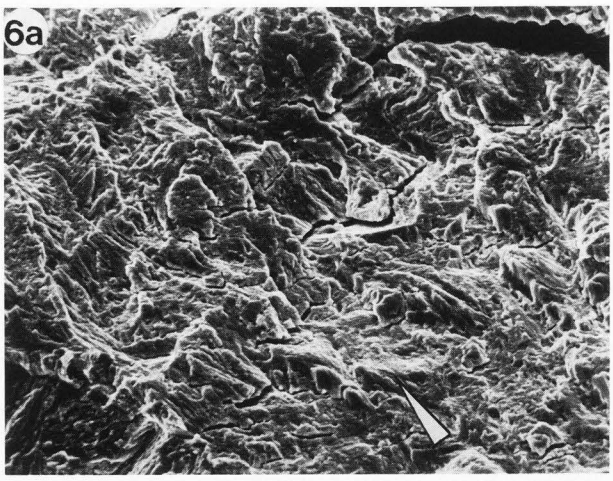

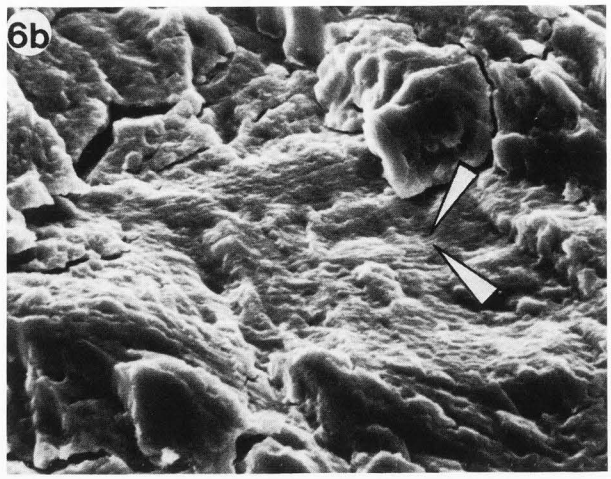

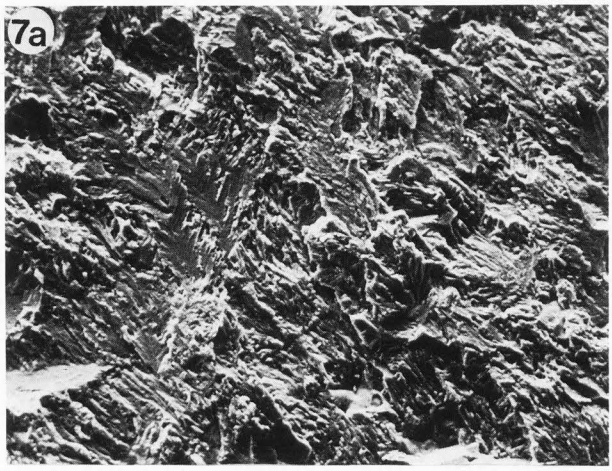

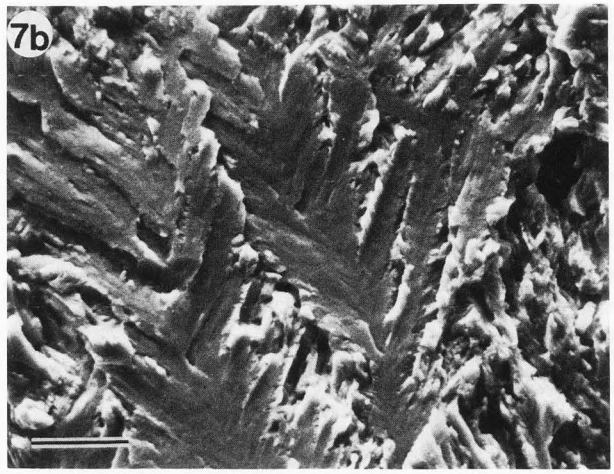

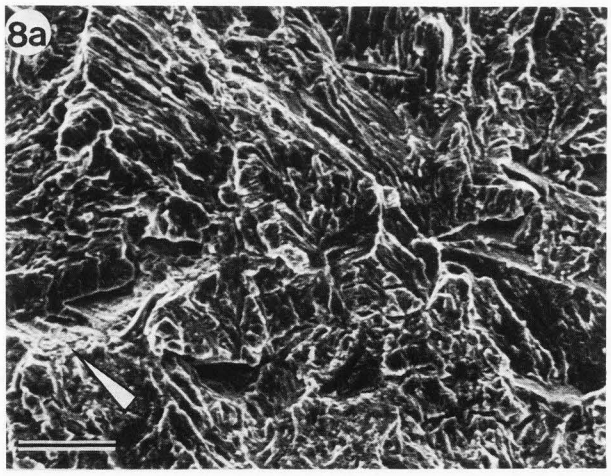

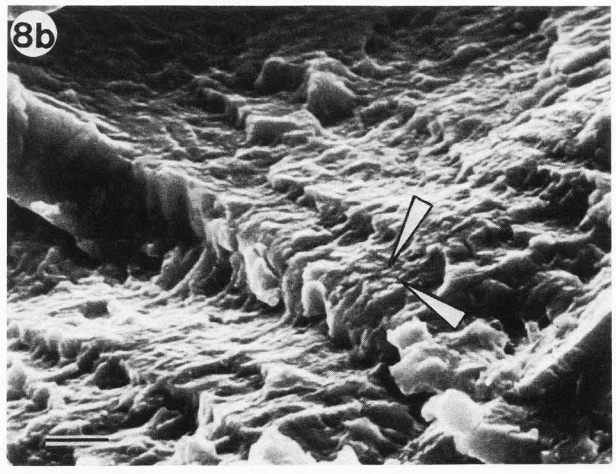

Figs. 6a and 6b: Fatigue striations (arrows) and secondary cracks at ΔK = 950 N/mm^{3}/^{2}, f = 1 Hz.
Figs. 7a and 7b: Fans and facets at ΔK = 350 N/mm^{3}/^{2}, f = 1 Hz .
Figs. 8a and 8b: Feathered structure, facets and fatigue striations (arrows) at ΔK = 550 N/mm^{3}/^{2}, f = 1 Hz.
Figs. 6, 7, and 8: Fracture characteristics as a function of ΔK-value at room temperature and R = 0.1 (fig. 6); 0.7 (figs. 7 and 8). Figs. 6a, 7a and 8a are at same magnification. Bar = 40 µm in fig. 8a. Figs. 6b and 7b are at same magnification, Bar = 10 µm in Fig. 7b. Bar = 2 µm in fig. 8b.

When the mean stress is increased, in the present investigations this was achieved by raising the stress ratio from R = 0.1 to 0.7, the respective fracture characteristics shift towards lower ΔK-value ranges.

At ΔK-values of the order of magnitude of 350 N/mm$^{3/2}$ and an R ratio of 0.1 a fracture structure is observed which is characterized by fans and isolated flat facets (Fig. 3). The fan vanes appear smooth; even at a magnification of 10,000 no fatigue striations can be discerned. The facets are formed by separation along crystallographic planes. A (111) orientation of these facets is to be assumed, according to previous investigations /8/. Their formation is considered to be part of the fatigue process and not as a rapid brittle fracture process. It is to be assumed that surfaces similar to "cleavage fracture surfaces" develop in the ductile austenitic material by alternate slip at crack tips in conjunction with the formation of very small voids ahead of the crack /3/; this mechanism is, however, not yet fully understood.

With the R ratio held constant at 0.1 "roughening" of the fan vanes to form discrete feathers starts in the ΔK-value range around 550 N/mm$^{3/2}$. The number of facets rises slightly and there are some secondary cracks (Fig. 4). The beginning of fatigue striation formation is to be discerned at magnifications of about 1,500 (striations indicated by arrows).

At a ΔK-value of 850 N/mm$^{3/2}$ (Fig. 5) the fracture structure appears feathered. In addition to facets and by this stage relatively clear fatigue striations, secondary cracks become much more evident.

As the ΔK-value is increased to 950 N/mm$^{3/2}$, fatigue striations are visible at magnifications as low as about 500 (Fig. 6). The number of secondary cracks rises, facets no longer occur.

The present data show that the higher the ΔK-value the better is the agreement between crack growth rate calculated from striation spacing and macroscopic crack growth rate.

There is nearly no effect of increased mean stress at low ΔK-values below 400 N/mm$^{3/2}$. Fans and facets are to be seen on the fracture surfaces, with the number of facets slightly larger and the fracture surface a bit more roughened at R = 0.7 than at R = 0.1 (compare Fig. 7 and Fig. 3).

By contrast a distinct difference in the fracture characteristics becomes visible at ΔK = 550 N/mm$^{3/2}$ and R = 0.7 compared with those of samples tested at identical range of the cyclic stress intensity factor but at R = 0.1. In addition to isolated facets, distinct fatigue striations occur in the feathered fracture structure of the sample tested at R = 0.7. These fracture characteristics resemble those of a fracture surface induced at 850 N/mm$^{3/2}$ and R = 0.1 (compare Fig. 8 and Fig. 5).

The fracture surfaces produced in demineralized water at a pressure of 30 bar and temperature of 200°C differ significantly from those in the room temperature samples. Facets are not observed, secondary cracks occur at low ΔK-values (Fig. 9). Featherings running in the direction of crack propagation and, above magnifications of about 1,500, fatigue striations are visible in the fans. The fans govern the appearance of the fracture surface at a magnification of about 500.

The number of secondary cracks and the distance between fatigue striations increase at higher ΔK-values (Fig. 10). At these ΔK-values of about 600 N/mm$^{3/2}$ the crack growth rate calculated from striation spacing is in good agreement with the macroscopic crack growth rate. (At lower ΔK-values the calculated crack growth rate is higher than the macroscopic one.)

No difference can be discerned between fracture surfaces induced at R = 0.2 and at 0.7 when ΔK-values are as low as 400 N/mm$^{3/2}$. At higher ΔK-values, i. e. 600 N/mm$^{3/2}$, a higher stress ratio makes itself somewhat more apparent in the form of wider secondary cracks, the longitudinal extension of which may be more than 100 µm. Furthermore, secondary micro-cracks of the order of magnitude of 1 µm occur between the individual fatigue striations.

Conclusions

In austenitic fracture surfaces produced in the tension-tension stress range at room temperature it is possible to distinguish four ranges of different fracture structure irrespective of test frequency and test environment. These ranges, in order of rising ΔK-value, are typified by the following characteristics: Range I: smooth to slightly roughened fans, facets, fatigue striations not discernible even at high magnifications; Range II: roughened fans or feathering on fracture surface, high proportion of facets, fatigue striations discernible at magnifications above approx. 1,500; Range III: feathered fracture structure, facets, fatigue striations and gaping secondary cracks visible at magnifications above approx. 500; Range IV: facets absent, distinct fatigue striations; secondary cracks.

These fracture ranges are correlated with ΔK-values and R ratio in the manner shown in Table 1.

This compilation shows that fracture features are the same whether they are caused by high ΔK-values and low R ratio or vice versa. So, the formation of fracture features is influenced decisively by the effective maximum stress.

The stress ratio also affects the crack growth rate at room temperature: as R increases from 0.1 to 0.7, the crack growth rate increases.

Fracture characteristics of samples tested at 200 °C differ from those tested at room temperature.

By contrast with the room temperature samples, however, no appreciable changes in fracture structure, i.e. appearance or disappearance of specific fracture features dependent on the ΔK-value, were observed in the samples tested at 200 °C. The effect of the R ratio on crack growth rate and fracture characteristics is only slight as well. Therefore, an estimation of the magnitude of the effective cyclic loading from fracture features is not possible within the range of ΔK-values (up to 600 N/mm$^{3/2}$) investigated.

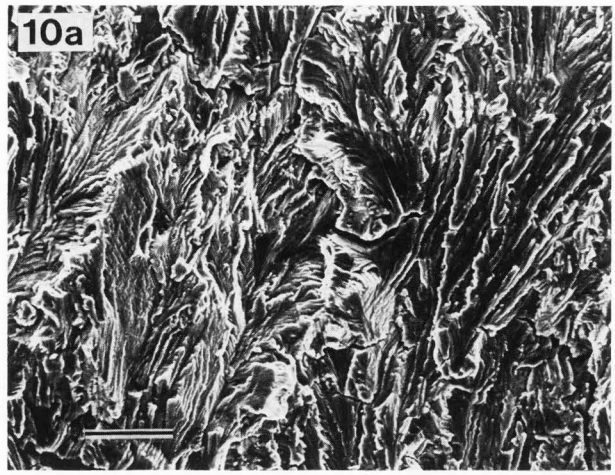

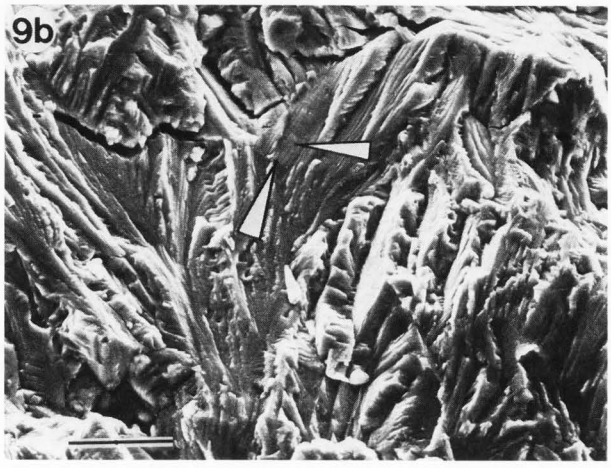

Figs. 9a and 9b: Fatigue striations (arrows) within a fan-like structure, secondary cracks at ΔK = 400 $N/mm^{3}/^{2}$, f = 0.1 Hz.
Figs. 10a and 10b: Fatigue striations (arrows) within a fan-like structure, secondary cracks at ΔK = 600 $N/mm^{3}/^{2}$, f = 0.1 Hz
Figs. 9 and 10: Fracture characteristics as a function of ΔK-value at T = 200 °C and R = 0.2.
Bar = 20 µm (in figs. 9a and 10a); 10 µm (in figs. 9b and 10b).

Table 1: Correlation between fracture characteristics, ΔK-value and stress ratio R at room temperature

Fracture characteristics	ΔK in $N/mm^{3}/^{2}$ at R = 0.1	ΔK in $N/mm^{3}/^{2}$ at R = 0.7
Smooth to rough fans, facets	< 400	< 400
Roughened fans or feathering, facets, fatigue striations at M = 1.500 x	400 to 800	400 to 550
Feathered, facets, fatigue striations at M = 500 x, gaping secondary cracks	800 to 900	550 to 650
Feathered, fatigue striations, secondary cracks	> 900	> 650

References

/1/ Burghard H. C., Davidson D. L. (1965). Fracture Mechanisms and Fracture Surface Topography, Int. Conference on Fracture, Sendai, B, 571 - 596, published by Japanese Society of Strength and Fracture of Materials.

/2/ Forsyth P. J. E. (1963). Fatigue Damage and Crack Growth in Aluminium Alloys, Acta Metallurgica, 11, 703 - 715.

/3/ Lynch S. P. (1981). Cleavage Fracture in Face-Centered Cubic Metals, Metal Science, 15, 463 - 467.

/4/ Masuda C., Nishijima S. (1982). Quantitative Analysis of Fatigue Fractographs for Some Heat Treated Steels, Transactions of National Research Institute for Metals, 24, 146 - 151.

/5/ Matzer F. (1982). Crack Growth in Steel under Cyclic Loading, Z. Werkstofftechnik, 13, 29 - 35.

/6/ McMinn A. (1981). Fractographic Analysis in the Understanding of Corrosion Fatigue Mechanisms, presented at IAEA Specialists' Meeting on Subcritical Crack Growth, Freiburg, May 13 to 15, 1981; published by Springfields Nuclear Power Development Laboratories, United Kingdom Atomic Energy Authority, Northern Division, 1 - 11.

/7/ Pelloux R. M. N., McMillan J. C. (1965). The Analysis of Fracture Surfaces by Electron Microscopy, Int. Conference on Fracture, Sendai, B, 547 - 569, published by Japanese Society of Strength and Fracture of Materials.

/8/ Priddle E. K., Walker F. E. (1976). The Effect of Grain Size on the Occurrence of Cleavage Fatigue Failure in 316 Stainless Steels, Journal of Material Science, 11, 386 - 388.

/9/ Schmitt-Thomas K.-H. G., Schulz H., Vollrath L. (1978). Influence of Different Bending Stress Collectives on the Fracture Features of Cylindrical Ck 45-Type Samples, VDI - Z (Verein Deutscher Ingenieure - Zeitschrift), 120, 145 - 152.

/10/ Taira S., Tanaka K. (1972). Fractography of Low-Carbon Steel in Fatigue Fracture, Journal of the Society of Materials Science, Japan, 21, 97 - 103.

/11/ Törrönen K., Hänninen H., Cullen W. H. jr. (1981). Mechanisms of Environment Assisted Cyclic Crack Growth in Nuclear Reactor Vessel Steels, presented at IAEA Specialists' Meeting on Subcritical Crack Growth, Freiburg, May 13 to 15, 1981, published by Technical Research Center of Finland, Espoo, 1 - 40.

/12/ Wessel E. T. (1968). State of the Art of the WOL Specimen for K_{Ic} Fracture Toughness Testing. Engineering Fracture Mechanics, 1, 77 - 103.

Discussion with Reviewers

G. Lange: Do you agree that "cleavage fracture surfaces" in austenitic material are the same phenomenon as the crystallographically orientated crack propagation in fatigue fracture of cobalt and nickel?

Authors: We think that formation of "cleavage fracture surfaces" in fatigue fractures is a general phenomenon of fcc materials.